Charge-state dependence of energy loss of MeV dimers in GaAs(100)

B. Sundaravel,* Christopher David, A. K. Balamurugan, S. Rajagopalan, A. K. Tyagi, B. K. Panigrahi, K. G. M. Nair, and B. Viswanathan

Materials Science Division, Indira Gandhi Center for Atomic Research, Kalpakkam 603102, India

(Received 21 November 2004; revised manuscript received 1 March 2006; published 25 April 2006)

Carbon and oxygen dimers with charge states 1+ and 3+ were implanted into GaAs along the [100] direction at an energy of 0.5 MeV/atom. The defect depth profiles are extracted from Rutherford backscattering spectrometry and channeling. The depth profile of carbon is extracted from secondary ion mass spectrometry measurements. The defect density produced by dimer ions is larger than monomer ions. The depth profile of carbon in dimer implanted GaAs is deeper than that of monomer implanted GaAs showing negative molecular effect. The defect depth profile of oxygen dimer implanted GaAs is deeper for 3+ than that for 1+ charge state. This indicates that energy loss of O_2^{3+} is smaller than that of O_2^+. It is attributed to charge asymmetry and a higher degree of alignment of O_2^{3+} along the [100] axis of GaAs.

DOI: 10.1103/PhysRevA.73.042902 PACS number(s): 34.50.Bw, 61.80.Lj, 61.85.+p

I. INTRODUCTION

The interaction of a cluster of n atoms is not a linear superposition of the interactions of n monomers due to the spatial and temporal close proximity of cluster-ion bombardment. The wake induced by one atomic constituent in a cluster ion modifies the retarding force acting on the other constituents and is called the vicinage effect. The vicinage effect has been investigated in various cluster impact phenomena such as damage production, energy loss, sputtering, secondary electron emission, crater or hillocks formation, latent tracks, etc. [1–5]. Brandt *et al.* [6] first found that the energy loss per hydrogen of 60–150 keV/atom hydrogen molecular ions is greater than the energy loss of hydrogen with equivalent velocity which is called the positive molecular effect. This vicinage effect tends to vanish as the relative distances grow up due to Coulomb explosion during their passage. The wake effect on the molecular-ion alignment with the incident beam direction was found by Gemmell *et al.* [7,8]. Eckardt *et al.* observed that the energy loss per atom of 12.5–130 keV/atom H_2^+ ions is less than that of H^+ with the same specific energy which can be called the negative molecular effect [9]. The negative molecular effect in heavier molecular ions N_2^+ and O_2^+ was reported by Steuer and Ritchie [10]. They explained the experimental data by taking into account the wake forces with the damping, internuclear separation, and parallel alignment of the molecule [10]. The alignment dependence of the energy loss of molecular ions has been estimated theoretically and it is found to be minimum when the internuclear axis is parallel to the incident beam direction [11,12]. Energy loss has been measured from channeling spectra of single crystals with hydrogen clusters. The positive molecular effect is observed for 250–800 keV/atom [13] of hydrogen ions in Si(111) and the negative molecular effect is observed for 7.5 keV/atom of hydrogen ions in Au(100) [14]. In addition to the energy, internuclear separation, and orientation of the cluster ions, their initial charge states (Q_1) can also influence the energy loss. In the energy loss process of monoatomic ions, the effects such as projectile excitation and ionization, charge equilibration and equilibrium charge states, energy loss by charge exchange, and nonlinear stopping had been studied [15–17]. For partially stripped ions the effective projectile charge (Z_{eff}) responsible for stopping depends on the impact parameter, approaching the nuclear charge Z_1e at small and the ion charge Q_1e at large impact parameters. The impact parameter of the ions will be large when they get channeled into a crystal. Also the charge state of the ion remains frozen as the ions are shielded from close encounters with lattice atoms and charge exchange probabilities are low. Only the screening effect of bound electrons is purely reflected in Z_{eff}. Golovchenko *et al.* have studied the charge-state dependence of the energy loss in the case of monomer atoms by implanting them along the channeling direction and found a $(Q_1e)^2$ dependence [18]. The vicinage effect on the average charge state of the emerging constituent ions of the cluster from thin carbon foils have been studied [19,20]. Reduction of the average charge state is observed and is attributed to the vicinage effect where the neighboring constituents create a perturbation of the atomic potential, which would result in a stronger binding of remaining electrons at each ion within the cluster and a theoretical model is given by Miskovic *et al.* [20]. There are no reports of a charge state dependence of energy loss of cluster ions. Here we report on the lattice damage and energy loss of diatomic carbon and oxygen ions with different charge states in semi-insulating GaAs(100).

II. EXPERIMENT

The GaAs(100) substrate is aligned with a 2-MeV He^+ beam from a 1.7-MV tandetron accelerator in our laboratory using an automated sample manipulator with three axes (x,y,z) of translation and two axes of rotation (θ,φ) [21]. After the alignment, carbon monomer (C^+) and dimer ions with various charge states and an energy of

*Electronic address: bsundar@igcar.gov.in

 ©2006 The American Physical Society

0.5 MeV/atom from the accelerator are implanted into GaAs substrates along the [100] direction at an atomic fluence of $4\times10^{14}/\mathrm{cm}^2$ and a flux of 8.85×10^{11} atoms/cm^2s. Samples have been prepared by implanting along random direction also. GaAs samples for oxygen implantation were implanted along the [100] direction at an atomic fluence of $8\times10^{14}/\mathrm{cm}^2$ with a flux of 6.6×10^9 and 6.6×10^{10} atoms/cm^2s. Carbon dimer ions are generated from a graphite target at the source of negative ions by cesium sputtering (SNICS) and injected into the accelerator. For oxygen dimers InO_2^- ions from In_2O_3 target at SNICS source are injected into the accelerator and O_2^{1+} and O_2^{3+} are selected after stripping of electrons by N_2 gas and second acceleration. One has to be aware of the stability of the clusters at higher charge states before doing the implantation. In our accelerator, the energy analyzing magnet cannot distinguish between ion species with the same m/Q ratio. This means that C_2^{+2} and C^+ emerging out of stripper canal of the accelerator cannot be distinguished. So for studying the charge state effects, we have used only 1+ and 3+ for the dimers. Carbon dimers up to charge states 3+ are shown to be stable by quantum mechanical calculations [22]. Even though carbon dimer with 3+ charge state has been shown to be stable theoretically, we could get only 1/1000th of C_2^+, i.e., 0.2 nA particle current on the sample which is not sufficient for performing the experiment. In oxygen we could get 1/100th of O_2^+, i.e., 1 nA particle current of O_2^{3+} on the sample and hence oxygen dimer implantation has been performed with O_2^+ and O_2^{3+}. For a uniform lateral distribution, the beam was rastered over the sample. As the defects produced in GaAs anneal out even at room temperature [23], ion channeling spectra with 2 MeV He^+ are taken in all the implanted samples at a fixed duration (3 h) after the implantation. A surface barrier detector with a resolution of 19 keV and at a scattering angle of 165° is used. The beam divergence is 0.05° during ion channeling measurements and within 0.4° during ion implantation. The calculated channeling half angle ($\psi_{1/2}$) [24] for the channeling of 0.5-MeV carbon ions along the [100] direction of GaAs is 1.87° which is much larger than the beam divergence and the beam is well channeled into the crystal.

Secondary ion mass spectrometry (SIMS) measurements in carbon implanted GaAs are taken using a CAMECA IMS-4F ion microscope. With a 3.3-keV Cs^+ primary beam, secondary positive ions of ^{12}C are detected. The Cs^+ beam current of 30 nA was rastered over an area of 150 μm$\times$150 μm. The secondary ions emitted from the central region (60 μm diameter) are collected by a sector type double focusing mass analyzer. The sputtering rate varied from 1.4 to 1.6 nm/s which is calculated by measuring the depth of the craters with a Dektak 6M Stylus profiler. Vacuum in the system during SIMS measurements is better than 1×10^{-9} Torr.

III. RESULTS AND DISCUSSION

Figure 1 shows the aligned Rutherford backscattering spectrometry (RBS) spectra of 2 MeV He^+ scattered from virgin and 0.5 MeV/atom C^+ and C_2^+ implanted GaAs(100) substrates with an atomic fluence of $4\times10^{14}/\mathrm{cm}^2$. The high-energy side of the spectra corresponds to backscattering from the surface and the yield is nearly the same for both the spectra at the surface. The ratio ($\chi_{\min}$) of the yield from the top surface for the aligned and random (not shown) spectra is a measure of the crystalline quality. For the virgin GaAs it is 3.7% which is close to the calculated value of 2.4% [24] and it indicates that the crystallinity is good. There is a peaking of yield around 960 keV (indicated by an arrow in Fig. 1) in the implanted samples which is due to the point defects caused by carbon implantation close to the projected range. The yield in the spectrum for C_2^+-implanted GaAs is larger than that in the spectrum of C^+-implanted GaAs which implies that dimer produces larger damage.

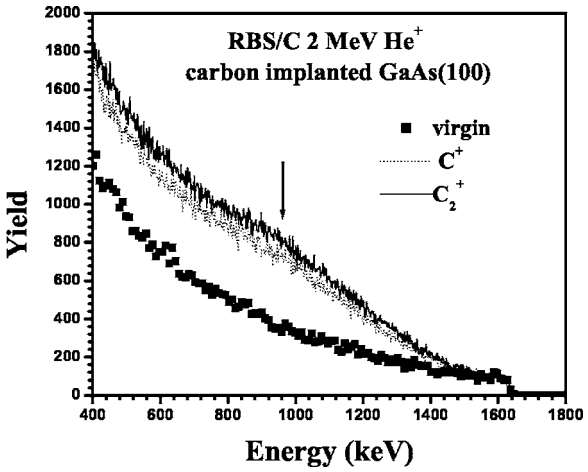

FIG. 1. RBS and channeling spectra of 2 MeV He^+ from virgin and 0.5 MeV/atom C^+, C_2^+ channeled implanted GaAs(100) substrates with an atomic fluence of $4\times10^{14}/\mathrm{cm}^2$.

Figure 2 shows the defect density depth profile extracted from the data in Fig. 1 by the following procedure. The random and aligned spectra of each sample in the implanted (D) and unimplanted (V) regions are converted to depth scale. The energy loss along the channeling direction can be as low as 0.5 times the value along the random direction. During the depth conversion, energy loss along the incident direction for

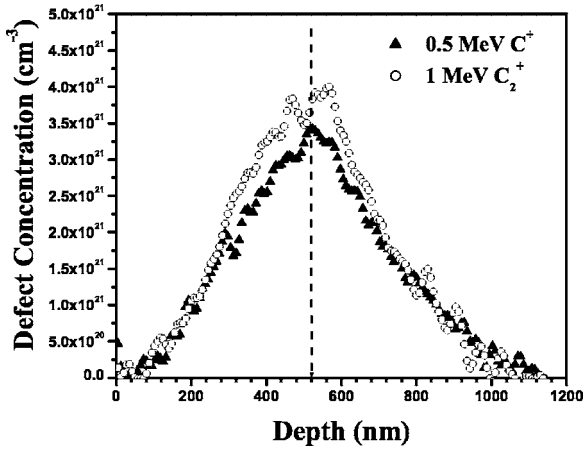

FIG. 2. Defect density depth profile extracted from the RBS and channeling spectra given in Fig. 1.

TABLE I. Parameters of the defect depth distributions of 0.5 MeV/atom carbon monomer and dimer at a fluence of 4×10^{14} atoms/cm^2 obtained from channeling spectra (The depth of the damage peaks (in nanometers) given are not absolute values as they can vary with the stopping multiplication factor used during depth conversion). The range and straggling (in nanometers) are obtained from SIMS data by fitting with a Gaussian function.

Species	Channeling implantation					Random implantation	
	Damage peak depth	Standard deviation	Defect density (10^{17}/cm^2)	Range	Straggling	Range	Straggling
C^+	519.1±3.3	201.9±5.9	1.60±0.07	974.7±2.2	164.8±3.3	839.8±2.9	154.7±3.8
C_2^+	510.6±2.8	196.0±4.6	1.83±0.07	977.5±1.7	165.6±2.2	852.8±2.5	151.9±2.9

the channeling spectra is assumed to be 0.7 (for virgin) and 0.8 (for implanted) times the value for the random incidence, while for the backscattered direction, it is taken as 1. After that the profile of the ratio of aligned to random yields for implanted (χ_D) and unimplanted (χ_V) regions of GaAs as a function of depth is obtained. The defect depth profile is obtained iteratively from $z=0$ using the following expression which is valid for a low density of defects [22]:

$$\chi_D(z) - \chi_V(z) \approx \frac{n_D(z)}{n} + \int_0^z \sigma_D n_D(z')dz'.$$

By fitting these curves with a Gaussian function, the damage peak depth, standard deviation, and total defect concentration are obtained and they are tabulated in Table I. The depth of the damage peaks given in Table I are not absolute values as they can vary with the stopping multiplication factor used during depth conversion. But they are good enough for comparison of the depths of the damage peaks due to different implanted species.

For 500-keV C^+ ions in GaAs, SRIM-2003 gives a projected ion range of 801 nm and a damage peak depth at 760 nm [25] and the observed defect depth values are smaller. After normalizing the defect peak area with respect to the incident ion fluence, we get 400 defects/ion for C^+-implanted GaAs while the SRIM-2003 value is 1272 displacements/ion [25]. The lower density of the defects is due to implantation along the axial direction as well as self-annealing of defects in GaAs. The defect density in C_2^+-implanted GaAs is larger than the defect density in C^+-implanted GaAs. Ghose *et al.* have observed that carbon dimers produce more lattice damage than carbon monomers with 1 MeV/atom in GaAs [26] when implanted along a random orientation. Our results show that it is valid when the ions are implanted along the [100] axial direction also at 0.5 MeV/atom. It is in agreement with the implantation studies of cluster ions in the channeling direction where an increase of the dechanneling rate caused by fragments of the Coulomb-exploded molecule over the transverse energy [27] has been reported. The increase of the dechanneling rate will cause an increase in the energy loss which in turn will give rise to a reduced projected range. This change should be reflected in our defect profile data of C^+ and C_2^+ implantations. But there is only a change of 10 nm in the depth of defect peaks and SIMS measurements are carried out for verifying the carbon depth profile.

Figure 3(a) shows the SIMS depth profile of carbon in GaAs implanted in channeling direction. Figure 3(b) shows the depth profile of carbon in samples implanted in random direction at a tilt angle of 7°. The data are fitted with a Gaussian and peak position and standard deviation are given in Table I. The SRIM-2003 value of range of the carbon ions in GaAs implanted at 7° for 500 keV is 801 nm. For the samples implanted with carbon at 7°, the measured range is very close to the SRIM-2003 value. Also the range of carbon in

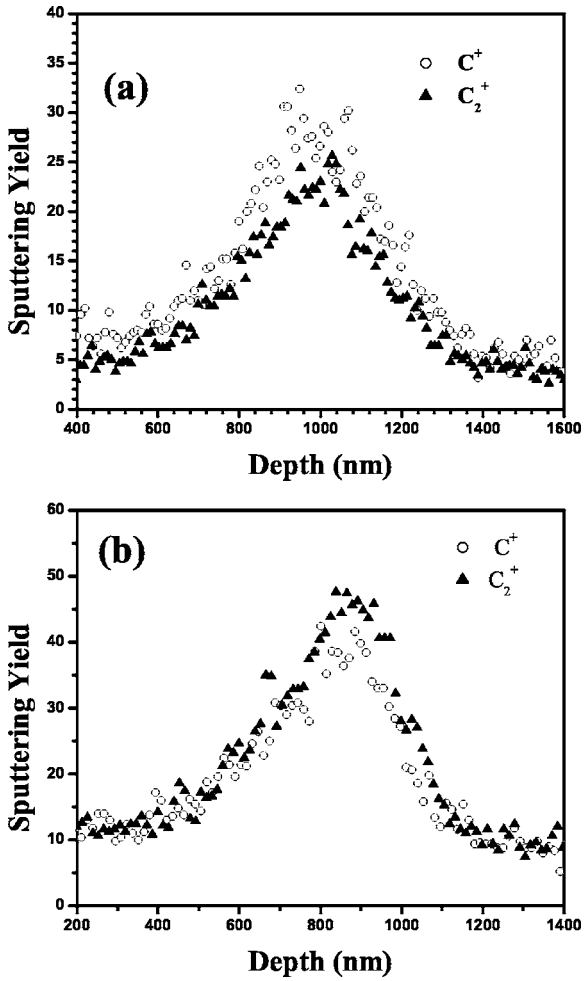

FIG. 3. The depth profile of carbon from SIMS measurements in GaAs implanted in (a) channeling direction and (b) random direction.

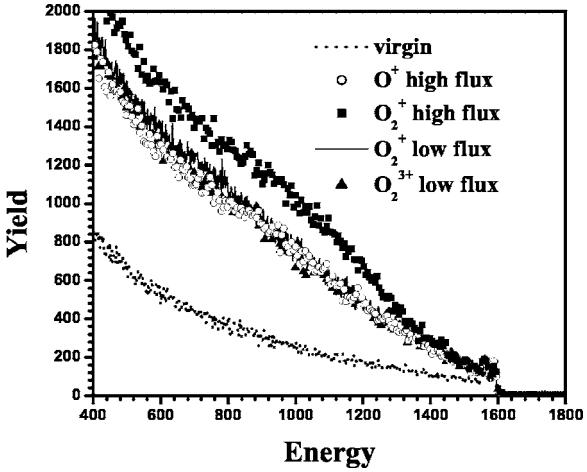

FIG. 4. RBS and channeling spectra of 2 MeV He^+ from virgin and 0.5 MeV/atom O^+, O_2^+ channeled implanted GaAs(100) substrates with an atomic fluence of $8\times10^{14}/cm^2$ at a flux of 6.6×10^9 atoms/cm^2s (low) and 6.6×10^{10} atoms/cm^2s (high).

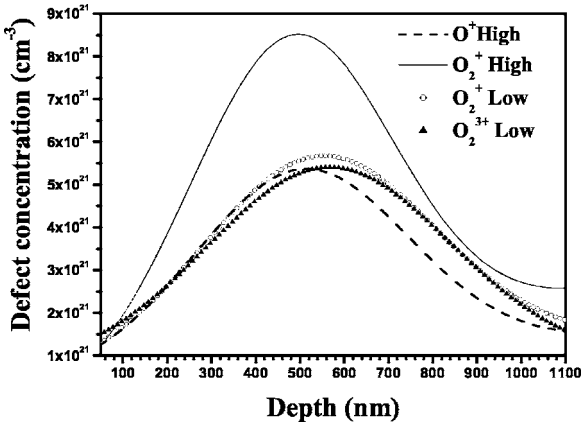

FIG. 5. Defect density depth profile extracted from the RBS and channeling spectra given in Fig. 4.

the dimer-implanted GaAs is deeper than that in the monomer-implanted GaAs, indicating negative molecular effect. Along channeling direction the energy loss is less which gives raise to deeper range (975 nm) and larger straggling. As the straggling is larger, difference in range between monomer and dimer is within the experimental error.

Figure 4 shows the channeling spectra with 2 MeV He^+ from virgin and O^+-, O_2^+-, and O_2^{3+}-implanted GaAs at two different ion fluxes. For a high flux, it is seen that yield is higher for the dimer implantation than the monomer implantation like in the case of carbon. For the dimer, the yield is larger for the high flux than the yield for a low flux. The defect profiles are extracted using the same procedure as in the case of carbon implanted GaAs. Figure 5 shows the Gaussian fit of defect profiles extracted from the spectra shown in Fig. 4. The parameters of the defect profiles are tabulated in Table II. For 500-keV O^+ ions in GaAs, SRIM-2003 gives a projected ion range of 705 nm and damage peak depth at 690 nm [25] and the observed defect depth values are smaller like in the case of carbon. After normalizing the defect peak area with respect to incident ion fluence, we get 313 defects/ion for O^+-implanted GaAs while the SRIM-2003 value is 1119 displacements/ion [25]. O_2^+ is showing larger damage and shallower damage peak position for the high flux implantation than the case of the low flux implantation at the same fluence. This observation is similar to the earlier reports on damage produced by monomer-implantation in GaAs [28]. It has been shown by molecular dynamics simulations that the range profile depends on the damage build up with the increase in fluence [29]. The lattice damage regardless of whether it is like individual defects or amorphous zones blocks channels and causes dechanneling of ions. Consequently the range profile changes shape towards the profile of a totally amorphous material. At lower ion flux, the lattice damage is less. Also defect buildup is slower and the ion could travel without dechanneling for a longer depth while it is opposite in the case of higher ion flux giving raise to the shallower damage peak. At lower ion flux, for the same ion fluence, O_2^{+3} is showing a deeper damage peak position than O_2^+, implying a reduced energy loss for the higher charge state of the dimer. Charge states can be preserved along the channeling axis and hence difference in range due to the change of charge state is observable in channeling-implanted samples.

The trajectories of the constituent atoms of a cluster ion inside a crystal are predetermined by the correlated initial conditions at the surface such as velocity, internuclear separation, and orientation of the internuclear axis. The internuclear separation in the carbon and oxygen dimers is between $2a_0$ and $3a_0$ (Bohr radius $a_0=0.0529$ nm) and the separation increases in carbon [20] and decreases in oxygen with an increase in the charge state. The energy loss of the dimers will vary with different internuclear separations as shown by Steuer and Ritchie using an extended Brandt-Kitagawa-model charge distribution [10]. At our incident velocities

TABLE II. Parameters of the defect depth distributions of 0.5 MeV/atom oxygen monomer and dimers with charge states 1+ and 3+ at a fluence of 8×10^{14} atoms/cm^2. (The depth of the damage peaks given are not absolute values as they can vary with the stopping multiplication factor used during depth conversion.)

Species	Flux (atoms/cm^2s)	Damage peak depth (nm)	Standard deviation (nm)	Total defect density (10^{17} defects/cm^2)
O^+	6.6×10^{10}	503.4±2.5	239.4±4.6	2.50±0.09
O_2^+	6.6×10^{10}	481.3±1.8	228.5±3.1	4.20±0.10
O_2^+	6.6×10^9	542.6±2.6	259.1±4.9	2.90±0.10
O_2^{3+}	6.6×10^9	563.9±3.2	273.2±6.3	2.90±0.14

($1.29v_0$ for C and $1.12v_0$ for O) the internuclear separation of the dimers is between $\hbar/2mv$ and v/ω_p where m, v, v_0, and ω_p are the mass of the monomer ion, ion velocity, Bohr velocity, and plasma frequency, respectively. Here the constituent ions in the cluster behave as separate ions with respect to the closest interactions with target electrons, while at the same time they behave as united ions with respect to the most distant collective interactions with adiabatic distance v/ω_p [2]. In the united atom limit, the stopping power ratio between the dimer and two individual monomers is 0.91 for carbon and 0.88 for oxygen using a simple model of Sigmund *et al.* [1]. This implies that a negative molecular effect is expected in both carbon and oxygen implantations and is consistent with the observed ion ranges in the implantation of carbon in GaAs.

Even though well-channeled particles retain charge-state stability, some of these ions will change charge. Due to wake effects in the dynamic interaction potential, the charge of the trailing ion in the cluster oscillates with increasing penetration depth, while the charge of the leading ion increases monotonically toward the value characteristic of an isolated ion at the same speed. This gives rise to ion charge asymmetry [26]. Dissociation of the cluster can be slowed down for longer penetration depths by charge state asymmetry [30]. O_2^{3+} may have higher ion charge asymmetry than O_2^+ and the initial correlations responsible for the negative molecular effect remain for a longer penetration depth.

The energy loss will be minimum when the internuclear axis is aligned with the incident beam direction even along a random direction in a crystal [10–12] and for the channeling direction, there should be a further reduction. As the reduction of energy loss is observed in the case of O_2^{3+}, it may have an easy aligning axis as in an analogous situation where the I_2 molecule aligns with the parallel component of the electric field of a laser only for charge states of 5+ or higher [31]. The electrostatic field is there inside the crystal also. The continuum potential is acting laterally and restricts the ion motion. The wake field is acting longitudinally and can align the internuclear axis with the beam direction [7,8]. The improved alignment with an increase in the charge states of O_2 can cause a longer penetration depth. The stability of the dimer combined with negative molecular effect can give rise to the slightly deeper ion ranges for higher charge states. Molecular dynamics simulations of Wang *et al.* show that a cluster can be stabilized against Coulomb explosion by varying its velocity [32]. Our experiment gives indirect evidence that cluster beam can be stabilized for longer duration by varying its initial charge state along channeling direction.

IV. CONCLUSION

Negative molecular effect is observed when carbon or oxygen dimers with 0.5 MeV/atom are implanted into GaAs. In channeling implanted samples charge state is preserved and the negative molecular effect increases with increase in charge state. This is attributed to change in internuclear separation, the alignment of the dimer axis with the beam direction and the stability of the dimer preserved by the transverse component of continuum potential of the GaAs crystal. Dechanneling of ions caused by coulomb explosion increases the energy loss while vicinage effect decreases the energy loss and there is a trade off between these two effects.

[1] P. Sigmund, I. S. Bitensky, and J. Jensen, Nucl. Instrum. Methods Phys. Res. B **112**, 1 (1996).

[2] N. R. Arista, Nucl. Instrum. Methods Phys. Res. B **164–165**, 108 (2000).

[3] S. Bouneau, A. Brunelle, S. Della-Negra, J. Depauw, D. Jacquet, Y. Le Beyc, M. Pautrat, M. Fallavier, J. C. Poizat, and H. H. Andersen, Phys. Rev. B **65**, 144106 (2002).

[4] J. Jensen, A. Dunlop, and S. Della-Negra, Nucl. Instrum. Methods Phys. Res. B **141**, 753 (1998).

[5] A. Colder, O. Marty, B. Canut, M. Levalois, P. Marie, X. Portier, S. M. M. Ramos, and M. Toulemode, Nucl. Instrum. Methods Phys. Res. B **174**, 491 (2001).

[6] W. Brandt, A. Ratkowski, and R. H. Ritchie, Phys. Rev. Lett. **33**, 1325 (1974).

[7] D. S. Gemmell, J. Remillieux, J. C. Poizat, M. J. Gaillard, R. E. Holland, and Z. Vager, Phys. Rev. Lett. **34**, 1420 (1975).

[8] D. S. Gemmell, J. Remillieux, J. C. Poizat, M. J. Gaillard, R. E. Holland, and Z. Vager, Nucl. Instrum. Methods **132**, 1342 (1976).

[9] J. C. Eckardt, G. Lantschner, N. R. Arista, and R. A. Baragiola, J. Phys. C **11**, L851 (1978).

[10] M. F. Steuer and R. H. Ritchie, Nucl. Instrum. Methods Phys. Res. B **33**, 170 (1988).

[11] J. Jensen, H. H. Mikkelsen, and P. Sigmund, Nucl. Instrum. Methods Phys. Res. B **88**, 191 (1994).

[12] T. Kaneko, Phys. Rev. A **51**, 535 (1995).

[13] M. Behar, P. L. Grande, G. de M. Azevedo, E. Alves, M. F. da Silva, and J. C. Soares, Nucl. Instrum. Methods Phys. Res. B **161–163**, 168 (2000).

[14] J. E. Valdés, C. Parra, C. Diaz-Valdés, C. O. Denton, C. Agurto, F. Ortega, N. R. Arista, and P. Vargas, Phys. Rev. A **68**, 064901 (2003).

[15] P. M. Echenique, F. Flores, and R. H. Ritchie, Solid State Phys. **43**, 229 (1990).

[16] P. Sigmund, Nucl. Instrum. Methods Phys. Res. B **69**, 113 (1992); Phys. Rev. A **50**, 3197 (1994); , **56**, 3781 (1997).

[17] P. Sigmund and L. Glazov, Nucl. Instrum. Methods Phys. Res. B **136–138**, 47 (1998).

[18] J. A. Golovchenko, A. N. Goland, J. S. Rosner, C. E. Thorn, H. E. Wegner, H. Knudsen, and C. D. Moak, Phys. Rev. B **23**, 957 (1981).

[19] A. Brunelle, S. Della-Negra, J. Depauw, D. Jacquet, Y. Le Beyec, and M. Pautrat, Phys. Rev. A **59**, 4456 (1999).

[20] Z. L. Miskovic, S. G. Davison, F. O. Goodman, W.-K. Liu, and Y. N. Wang, Phys. Rev. A **61**, 062901 (2000).

[21] K. Suresh, B. Sundaravel, B. K. Panigrahi, K. G. M. Nair, and B. Viswanathan, Rev. Sci. Instrum. **75**, 4891 (2004).

[22] Z. H. Zhu and R. Wang, Chin. Phys. **12**, 1218 (2003).

[23] R. P. Sharma, R. Bhadra, L. E. Rehn, P. M. Baldo, and M. Grimsditch, J. Appl. Phys. **66**, 152 (1989).
[24] L. C. Feldman, J. W. Mayer, and S. T. Picraux, *Materials Analysis by Ion Channeling* (Academic Press, New York, 1982).
[25] J. F. Ziegler, J. P. Biersack, and U. Littmark, *The Stopping and Ranges of Ions in Solids* (Pergamon, New York, 1985).
[26] S. K. Ghose, G. Kuri, Amal K. Das, B. Rout, D. P. Mahapatra, and B. N. Dev, Nucl. Instrum. Methods Phys. Res. B **156**, 125 (1996).
[27] V. A. Khodyrev, V. S. Kulikauskas, and C. Yang, Nucl. Instrum. Methods Phys. Res. B **195**, 259 (2002).
[28] R. A. Brown and J. S. Williams, J. Appl. Phys. **81**, 7681 (1997).
[29] J. Peltola, K. Nordlund, and J. Keinonen, Nucl. Instrum. Methods Phys. Res. B **195**, 269 (2002).
[30] H.-W. Li, Y.-N. Wang, and Z. L. Miskovic, Nucl. Instrum. Methods Phys. Res. B **193**, 204 (2002).
[31] Ch. Ellert and P. B. Corkum, Phys. Rev. A **59**, R3170 (1999).
[32] Y.-N. Wang, H.-T. Qiu and Z. L. Miskovic, Phys. Rev. Lett. **85**, 1448 (2000).